Simulation study of the polarizable Stockmayer fluid in an external field

Ran Jia and Reinhard Hentschke*

Fachbereich Mathematik und Naturwissenschaften, Bergische Universität, D-42097 Wuppertal, Germany

(Received 17 August 2011; revised manuscript received 27 October 2011; published 28 November 2011)

Gas-liquid phase coexistence curves of the polarizable Stockmayer fluid in external electric fields are computed using molecular dynamics computer simulation. We study in particular the critical-point shift dependence on polarizability and external electric field distinguishing the cases of fixed charge density and fixed potential. The results are compared to a previously developed mean-field theory for the polarizable Stockmayer fluid in an external field. We also investigate the behavior of the isochoric heat capacity near gas-liquid criticality via finite-size scaling depending on polarizability and external field.

DOI: 10.1103/PhysRevE.84.051508 PACS number(s): 64.70.F−, 68.35.Rh, 87.10.Tf, 64.75.Gh

I. INTRODUCTION

The Stockmayer potential, which consists of a Lennard-Jones (LJ) potential plus a point dipole–point dipole interaction, where the dipole moments are located on the Lennard-Jones sites, is one of several early potentials invented as models for small polar molecules [1]. Subsequently, numerous computer simulations have revealed its perhaps unexpectedly complex phase behavior. It does not reproduce real fluids of small polar molecules very well, e.g., its ferroelectric ordering transition appears to have no analog in real low molecular weight liquids [2], but it is still useful because its simplicity allows insight into the role of dipolar interactions for many structural, dynamic, and thermodynamic properties of liquids [3,4]. Here we present computer simulation results for the Stockmayer potential in an electric field including an induced point polarizability as continuation of a previous study of the nonpolarizable Stockmayer (ST) fluid in an electric field near criticality [5].

Although a simulation algorithm for the polarizable Stockmayer (pST) model is described in the early papers by Vesely [6,7], initially this model and related dipolar fluid models were not studied frequently due to the complexity of the calculations. Carnie and Patey [8] derived a self-consistent mean-field theory to study polarizable hard-sphere particles with embedded point dipoles and tetrahedral quadrupoles. Subsequently Caillol *et al.* [9] and Patey *et al.* [10] compared this theory to molecular dynamics (MD) results for thermodynamic and dielectric properties of polarizable Lennard-Jones particles with permanent dipole and quadrupole moments. At the same time Neumann and Steinhauser [11] developed a set of equations describing the dependence of the dipole-moment fluctuations on boundary conditions in computer simulations of isotropically polarizable polar systems. Mooil and co-workers [12,13] reported results of MD simulations of mixtures containing nonpolarizable ST and polarizable LJ particles using the Ewald summation to evaluate the dipolar interactions. They presented thermodynamic and structural properties, including the dielectric constants of the polarizable polar fluids obtained via the polarization fluctuations of the simulation cell. Similarly thermodynamic properties of the pST fluid were studied via MD simulations and perturbation theory by Kriebel and Winkelmann [14]. Millot *et al.* [15] performed extensive MD studies, comparing different methods for the evaluation of the long-range interactions, of the static dielectric constant in the pST fluid. Valiskó [16,17] reported the studies of the dielectric constant of the pST and dipolar hard-sphere (DHS) fluids using the Monte Carlo (MC) simulation in conjunction with renormalized perturbation theory. Most recently Moučka [18] developed a biased multiparticle MC scheme to study systems with nonadditive interactions using the pST fluid as the test system. Only a few studies have focused on gas-liquid phase coexistence of polarizable polar fluids. Kriebel and Winkelmann [19] studied the gas-liquid equilibria of ST fluids with fixed and polarizable dipoles using a perturbation theory. They conclude that the critical densities increased slightly as polarizability increases. Using grand canonical MC, Kiyoharaet *et al.* [20] investigated the phase coexistence properties of pST fluids with dipole moments $\mu = 1,2$ and point polarizabilities $\alpha = 0.00$, 0.03, and 0.06, but in the absence of an external field. They find that the critical temperature as well as the critical density increase with increasing polarizability.

In this paper we present our simulation results for the pST systems with dipole moments μ from 0.5 to 2.0 and point polarizabilities α from 0.0 to 0.08 (the conversion to SI units is explained at the beginning of the results section) in external electric fields. Using the MD simulation technique we compute gas-liquid phase coexistence curves. We study, in particular, the critical-point shift dependence on polarizability and external electric field distinguishing the cases of fixed external charge density or fixed potential. The results are compared to a previously developed mean-field theory for the polarizable Stockmayer fluid in an external field. In addition, we study the isochoric heat capacity near gas-liquid criticality via finite-size scaling, depending on polarizability and external field. For vanishing external field we find Ising behavior, whereas for nonvanishing external fields we find a significantly reduced (enhanced) critical exponent ratio α/ν when the potential (charge density) is fixed.

II. METHODOLOGY

The general MD simulation method for the pST fluid in an external electric field is described in Ref. [5]. However, for

*hentschk@uni-wuppertal.de;
http://constanze.materials.uni-wuppertal.de

reasons of transparency, we reproduce the key equations. The total potential energy of the system is

$$U = U_{\rm LJ} - \frac{1}{2}\vec{m}_i \mathbf{T}_{ij}\vec{m}_j - \frac{1}{2}\vec{m}_i \cdot g\vec{M}_i + \frac{1}{2}\frac{\vec{p}_i{}^2}{\alpha} - \vec{m}_i \cdot \vec{E}_i^{\rm ext} \tag{1}$$

(making use of the summation convention). Here $U_{\rm LJ}$ includes all LJ pair potentials between ST particles i and j. The other terms describe the interactions between point dipole moments $\vec{m}_i = \vec{\mu}_i + \vec{p}_i$ located on every site i. $\vec{\mu}_i$ is a permanent point dipole moment, and $\vec{p}_i = \alpha\vec{E}_i$ is an induced point dipole moment, where α is a site polarizability and $\vec{E}_i = \mathbf{T}_{ij}\vec{m}_j + g\vec{M}_i + \vec{E}_i^{\rm ext}$ is the total electric field at site i. The quantity $\mathbf{T}_{ij}$ is the dipole tensor, and $\vec{E}_i^{\rm ext}$ is the external field as it is felt at site i. The external field is assumed to be constant throughout the volume V of the system. However, we keep the index i as a reminder that the relation between a true external field $\vec{E}^{\rm ext}$, e.g., generated by capacitor plates between which the system is placed, and $\vec{E}_i^{\rm ext}$ does depend on how long-range interactions are handled in the simulation.

We use a cutoff $r_{\rm cut}$ centered on each particle. Inside the cutoff all pair interactions are computed explicitly. In the case of the LJ interactions we employ the usual continuum approximation for the interaction of the central site with particles outside the cutoff. The electrostatic effects on dipole i due to dipoles beyond $r_{\rm cut}$ are included in the reaction field approximation via the terms $-\frac{1}{2}g\vec{m}_i \cdot \vec{M}_i$ in Eq. (1) and $g\vec{M}_i$ in the formula for $\vec{E}_i$. Here $g = \frac{2(\epsilon-1)}{(2\epsilon+1)}\frac{1}{r_{\rm cut}^3}$ and $\vec{M}_i$ is the total dipole moment of the cutoff sphere surrounding particle i. ϵ is the static dielectric constant in the system under given conditions computed via

$$\frac{(\epsilon-1)(2\epsilon+1)}{9\epsilon}\vec{E}_i^{\rm ext} = \frac{1}{r_{\rm cut}^3}\langle\vec{M}_i\rangle. \tag{2}$$

The reaction field method here has the particular appeal that it may be compared to analytic results if there is only one dipole in the spherical cutoff. For instance, Eq. (1) may by rationalized by considering a single point dipole at the center of a spherical cavity in a dielectric medium. For a permanent dipole moment the potential energy consists of $-\vec{\mu}\cdot\vec{E}_{\rm cav}$ plus $-(1/2)\vec{\mu}\cdot\vec{E}_{\rm reac}$, where $\vec{E}_{\rm cav} = 3\epsilon\vec{E}^{(\infty)}/(2\epsilon+1)$ is the cavity field and $\vec{E}_{\rm reac} = g\vec{\mu}$ is the reaction field. $\vec{E}^{(\infty)}$ is the average electric field far from the cavity (Maxwell field). This calculation can, for instance, be found in Fröhlich's book [21]. If a polarizability α is added to the dipole moment then a third term $-(1/2)\vec{p}\cdot(\vec{E}_{\rm cav}+\vec{E}_{\rm reac})$ must be added to the dipole's potential energy, i.e., $u_D = -\vec{\mu}\cdot\vec{E}_{\rm cav} - (1/2)\vec{\mu}\cdot\vec{E}_{\rm reac} - (1/2)\vec{p}\cdot(\vec{E}_{\rm cav}+\vec{E}_{\rm reac})$. Rearrangement of terms yields $u_D = -(1/2)\vec{m}\cdot g\vec{m} + (1/2)\vec{p}^2/\alpha - \vec{m}\cdot\vec{E}_{\rm cav}$—the one-dipole analog of Eq. (1).

In particular, we note that $\vec{E}_i^{\rm ext}$ corresponds to $\vec{E}_{\rm cav}$. In the present simulation the cavity is the cutoff sphere embedded in a homogenous slab of dielectric material. This dielectric is thought to fill the space between the perpendicular (infinite) plates of a capacitor. And thus

$$\vec{E}_i^{\rm ext} = \frac{3\epsilon}{2\epsilon+1}\vec{E}^{(\infty)}. \tag{3}$$

The average field inside the dielectric in turn is related to an external field via $\vec{E}^{\rm ext} = \epsilon\vec{E}^{(\infty)}$. $\vec{E}^{\rm ext}$ is the field in a narrow (and therefore otherwise negligible) gap between one of the capacitor plates and the dielectric. Notice that two scenarios are particular relevant: (i) fixed charge density on the capacitor plates and (ii) fixed potential. Case (i) corresponds to $\vec{E}^{\rm ext}$ held constant. This follows from Gauss's law applied to the boundary between the capacitor plates and the adjacent gap. Case (ii) corresponds to $\vec{E}^{(\infty)}$ held constant. This follows directly via $\vec{E}^{(\infty)} = -\vec{\nabla}\varphi$, where φ is the scalar potential.

Additional quantities derived via the total potential energy are the force and the torque on particle i [see Eqs. (9) and (10) in Ref. [5]] and the pressure $P = P_{\rm LJ} - \frac{1}{2V}\langle\vec{m}_i\mathbf{T}_{ij}\vec{m}_j\rangle + P_\epsilon$, where P_ϵ is given by

$$P_\epsilon = -\frac{3\rho}{V}\left\langle\frac{1}{(2\epsilon+1)^2}\left(\vec{m}_i\cdot\vec{A}_i + \frac{\vec{m}_i\cdot\vec{M}_i}{r_{\rm cut}^3}\right)\frac{\partial\epsilon}{\partial\rho}\right\rangle, \tag{4}$$

with $\vec{A}_i = \vec{E}^{(\infty)}$ if $E^{(\infty)}$ is held constant and $\vec{A}_i = -2\vec{E}^{\rm ext}$ if $E^{\rm ext}$ is held constant instead. We note that potential energy, force, torque, and virial, in the absence of the external field, were worked out by Vesely [6]. We note also that our expression for the reaction field contribution to the pressure differs from the corresponding contribution in Vesely's work, because of the neglect of the density dependence of ϵ in the aforementioned reference.

The equations of motion are integrated using the velocity Verlet algorithm. Temperature, which is in LJ units here, is controlled via the weak-coupling method of Berendsen *et al.* [22]. Induced dipole moments are calculated at every MD step using the iteration scheme $\vec{p}_i{}^{(k+1)} = \alpha\vec{E}_i(\vec{p}_i{}^{(k)})$. The dielectric constant is calculated via Eq. (2). Gas-liquid (g-l) phase coexistence curves are obtained by the same method as introduced previously [23,24], i.e., phase coexistence is established using the Maxwell construction method applied to simulation isotherms at different temperatures. The number of Stockmayer particles N and the long-range cutof, $r_{\rm cut}$ are 900 and 5.5, respectively, unless explicitly noted otherwise. Notice that tests with larger cutoffs up to 7.5 do not yield significantly different results.

In the following the simulation results are compared to a simple mean-field description of the g-l transition developed previously [5]. The relevant free energy is $\Delta F = \Delta F_D + \Delta F_{\rm vdW}$, with

$$\frac{\Delta F_D}{NT} = -\ln\left(\frac{\sinh[K]}{K}\right) - \frac{1}{2(1-\alpha g)T}\left(g\mu^2 + \alpha E_{\rm cav}^2\right), \tag{5}$$

where $K = \mu E_{\rm cav}/[(1-\alpha g)T]$, and

$$\frac{\Delta F_{\rm vdW}}{NT} = \ln\left(\frac{\rho/\left(3\rho_c^o\right)}{1-\rho/\left(3\rho_c^o\right)}\right) - \frac{9}{8}\frac{\rho/\left(3\rho_c^o\right)}{T/\left(3T_c^o\right)}. \tag{6}$$

Here the first term in Eq. (5) accounts for the entropy loss due to orientation in the field, and ρ_c^o and T_c^o in Eq. (6) refer to the critical point of the pure LJ system ($\rho_c^o = 0.3$ and $T_c^o = 1.32$). Notice that the dielectric constant entering through the quantity g is computed via Eq. (A13) in Ref. [5]. Notice also that the quantity $r_{\rm cut}$ in g has two different meanings. In the simulation $r_{\rm cut}$ is the usual cutoff distance, whereas in the mean-field

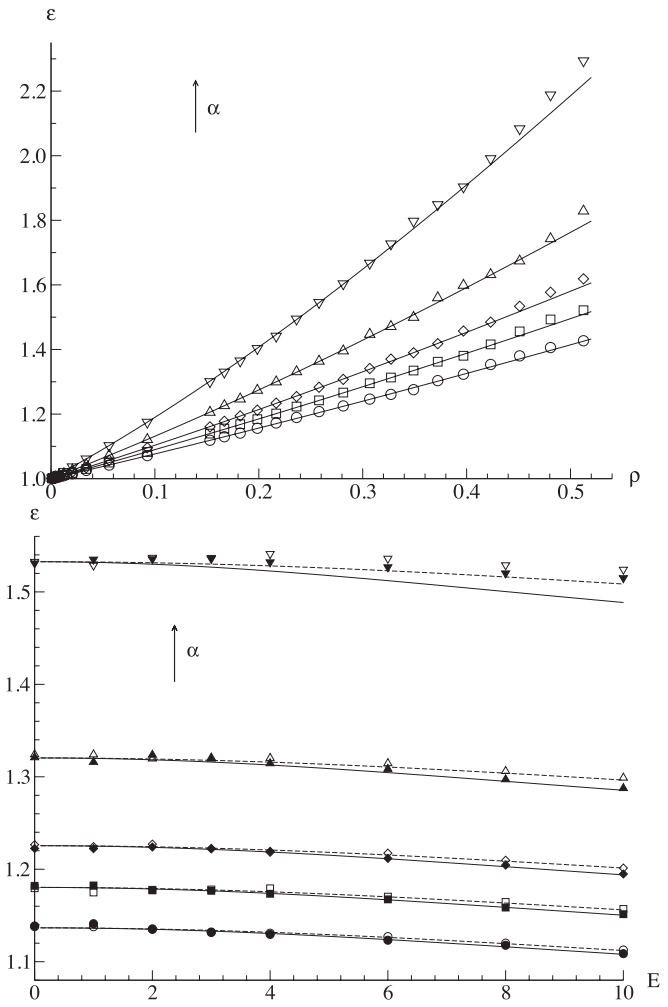

FIG. 1. Top: Static dielectric constant ϵ vs dipole number density ρ for $\mu = 0.5$, $T = 1.40$, and $E_i^{\rm ext} = 0$. Symbols: simulation results (circles: $\alpha = 0$; squares: $\alpha = 0.01$; diamonds: $\alpha = 0.02$; up triangles: $\alpha = 0.04$; down triangles: $\alpha = 0.08$); lines: mean-field theory. Bottom: ϵ vs field strength E for $\mu = 0.5$, $T = 2.50$, and $\rho = 0.313$. The correspondence between symbol shapes and α is the same as above. Note that ϵ at $E = 0$ is computed using Eq. (9) in Ref. [25]. The lines are computed via mean-field theory. Solid symbols and solid lines: $E = E^{(\infty)}$; open symbols and dashed lines: $E = E^{\rm ext}$.

theory $r_{\rm cut}$ is the radius of the cavity containing just one dipole. In this latter case we use $r_{\rm cut} = 0.8$ (as used previously in Ref. [5]).

III. RESULTS

The upper panel in Fig. 1 shows an example of the density dependence of the static dielectric constant ϵ obtained from the simulations compared to corresponding mean-field results. The static dielectric constant increases, as expected, when the point polarizability of the ST particle increases. Notice that, for example, the polarizability of water is $\sim 1.45 \times 10^{-24}$ cm^3. We may convert this number to the current units by multiplication with σ^{-3}, where σ is the LJ parameter, which, depending on the water model used, varies between 3.154 Å in the case of the simple point charge/extended (SPC/E) water model to 2.65 Å for an older Stockmayer water model. For α one obtains either 0.046 or 0.08, values in the α range considered here. The same is true for other small molecules. The permanent dipole moment in SI units may be obtained via $\mu\sqrt{4\pi\epsilon_o\epsilon\sigma^3}$. Here ϵ_o is the vacuum permittivity and ϵ and σ are LJ parameters. For example, choosing $\mu = 1$, $\epsilon/k_B = 380$ K, and $\sigma = 2.65$ Å (Stockmayer water) yields $\approx 1D$. Finally, the electric field in SI units expressed via the electric field in this work E is $\sqrt{\epsilon/(4\pi\epsilon_o\sigma^3)}E$.

The lower panel in Fig. 1 compares external field effects for nonpolarizable ST and four different pST fluids when either $E^{(\infty)} = \text{const}$ or $E^{\rm ext} = \text{const}$. The temperature and density are close to the respective critical values for nonpolarizable ST with $\mu = 0.5$ at zero field. The mean-field theory is a good description of the electric field dependence of ϵ. Significant discrepancies only occur at the highest polarizability, where structural correlations in the liquid are much stronger. One example is the formation of reversible aggregates, as chains (cf., for instance, Ref. [23]), which we try to avoid here due to the additional complexity.

Figure 2 shows the critical temperature ratio $T_c/T_c^{\alpha=0}$ and the critical density ratio $\rho_c/\rho_c^{\alpha=0}$ as functions of polarizability α for different values of the permanent dipole moment μ at zero-field strength. Increasing α or μ shifts the critical temperature to higher values. Our results are in very good agreement with the older values obtained in Ref. [20], where the authors use the histogram reweighting method to determine the critical parameters. The star symbols show results obtained via the renormalized perturbation theory in Ref. [19] for $\mu = \sqrt{2}$. Even though no simulations were carried out with this μ value, the result appears to be at least consistent with the simulations. Our own mean-field theory describes $T_c/T_c^{\alpha=0}$ vs α only qualitatively. In the case of the critical density ratio $\rho_c/\rho_c^{\alpha=0}$ the results are less straightforward. This is because computational errors are quite substantial. Nevertheless, for the dipole moments 1.0 and 2.0 the critical density increases. This is consistent with the theoretical result in Ref. [19]. It also appears consistent with the simulation results in Ref. [20], even though the errors of the critical density values are considerable. In the case of our smallest μ value, $\mu = 0.5$, we find a slight decrease of the critical density with increasing polarizability. This is in accord with our mean-field theory, which in this case also yields a good prediction of the T_c shift. However, our mean-field theory fails to describe the apparent increase of ρ_c for the larger dipole moments. Because this is the only case where thus far we have found a qualitative discrepancy between the simulation and this simple mean-field theory, including also our previous results for $\alpha = 0$ in Ref. [5], we conclude that structural correlations, absent in the mean-field description, are a likely cause for the disagreement. Notice that the numerical data of Fig. 2 are compiled in Table I.

Figure 3 shows selected gas-liquid coexistence curves obtained via MD simulations in conjunction with the Maxwell's construction method described in Ref. [5] for $\mu = 0.5$, $\alpha = 0.01$ and $\mu = 1.0$, $\alpha = 0.04$. A complete listing of our values for $\Delta T_c = T_c(\mu,E,\alpha) - T_c(\mu,0,\alpha)$ and $\Delta\rho_c = \rho_c(\mu,E,\alpha) - \rho_c(\mu,0,\alpha)$, where $E = E^{(\infty)}$ or $E = E^{\rm ext}$, is compiled in Tables II and III for $\mu = 0.5$ and 1.0, respectively. Notice that the overall comparison of the critical temperature shifts between the simulation results and the mean-field theory is

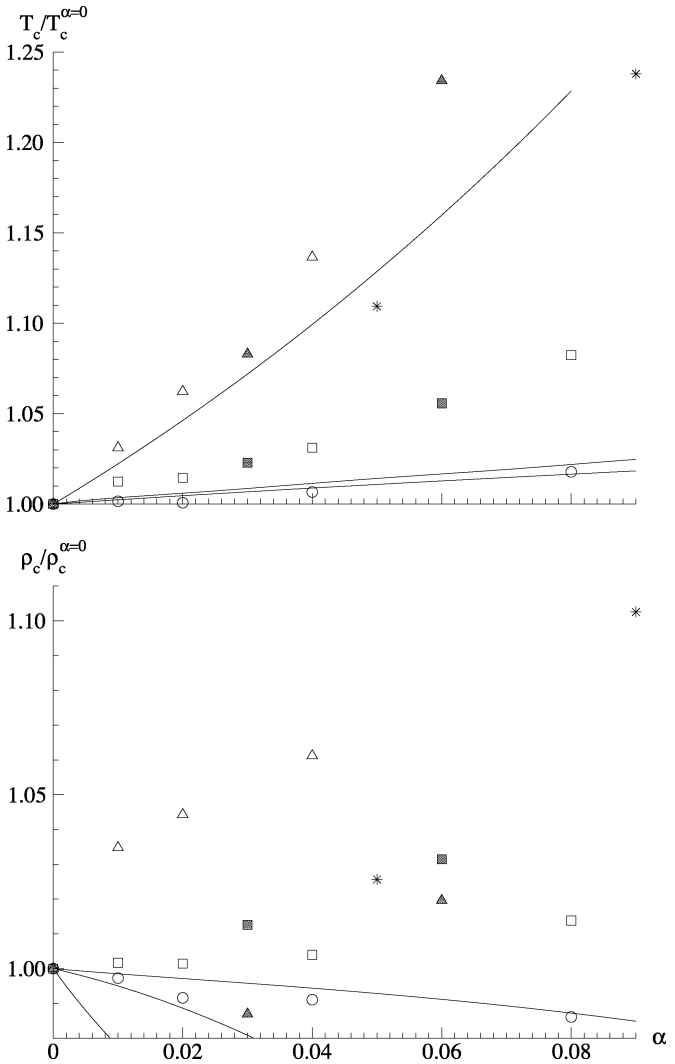

FIG. 2. Top: Simulated critical temperature T_c in units of the critical temperature of the corresponding nonpolarizable system $T_c^{\alpha=0}$ vs polarizability α. Open circles: $\mu = 0.5$; open squares: $\mu = 1.0$; open triangles: $\mu = 2.0$; solid squares and solid triangles: $\mu = 1.0$ and $\mu = 2.0$ from Ref. [20]; stars: $\mu = \sqrt{2}$ from Ref. [19]; lines: mean-field theory. Bottom: Corresponding critical density ρ_c in units of the critical density of the corresponding nonpolarizable system $\rho_c^{\alpha=0}$ vs α.

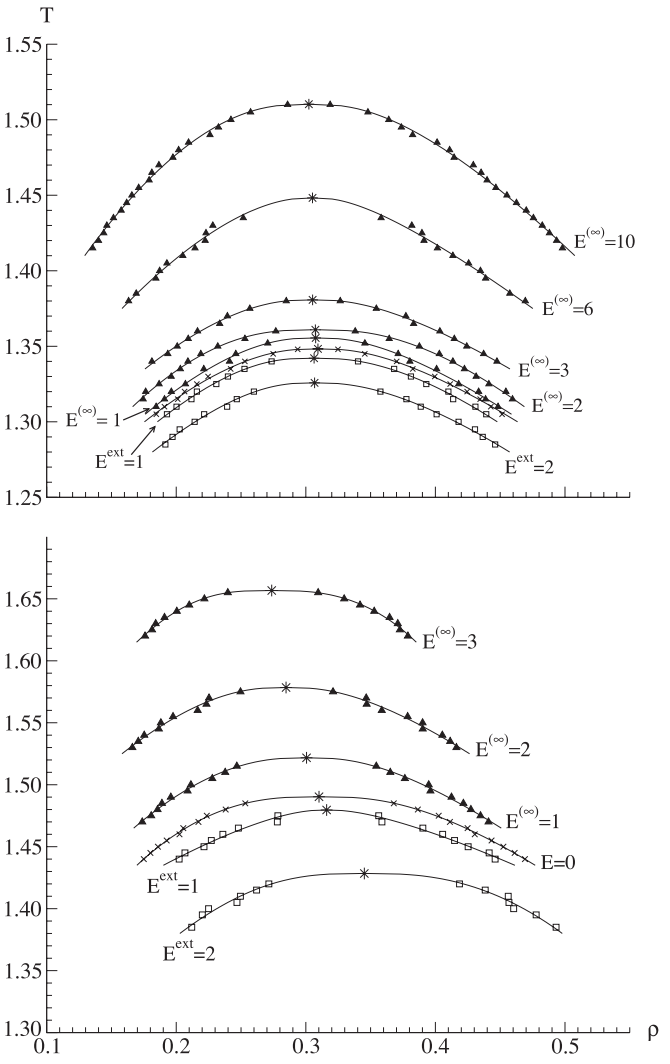

FIG. 3. Gas-liquid coexistence curves in the temperature-number density-plane based on simulated isotherms. Top: $\mu = 0.5, \alpha = 0.01$; bottom: $\mu = 1.0$, $\alpha = 0.04$. Stars denote critical points. Crosses: zero external field; triangles: $E^{(\infty)}$ is held constant; squares: E^{ext} is held constant. The statistical error is comparable to the size of the symbols.

quite good. An example plot of the reduced mean-field critical temperature and the critical density shift for $\mu = 0.5$ is shown in Fig. 4, together with corresponding simulation results.

TABLE I. The simulated critical temperatures and densities for pST systems with $\mu = 0.5$, 1.0, 2.0, and zero external field.

α		0	0.01	0.02	0.04	0.08
$\mu = 0.5$	T_c	1.346	1.348	1.347	1.355	1.370
	ρ_c	0.310	0.309	0.308	0.307	0.306
$\mu = 1.0$	T_c	1.445	1.463	1.466	1.490	1.564
	ρ_c	0.309	0.309	0.309	0.310	0.313
$\mu = 2.0$	T_c	2.087	2.152	2.217	2.372	–
	ρ_c	0.269	0.278	0.281	0.286	–

Simulation results for $E = E^{\text{ext}}$ at large field strengths are not included, because the simulation snapshots appear rather inhomogeneous, indicating the formation of reversible aggregates and possible structure formation thereof (such as bundle formation). We note that the signs of ΔT_c and $\Delta\rho_c$ depend on which field, $E = E^{(\infty)}$ or $E = E^{\text{ext}}$, is held constant. This is explained in detail in our previous paper [5]. For constant E^{ext}, the orientation contribution to free energy f_{orient} increases with increasing density, which in turn diminishes the van der Waals loop in comparison to the zero-field case, i.e., ΔT_c is negative. On the other hand, when $E^{(\infty)}$ is held constant, f_{orient} decreases with increasing density, which in turn enhances the van der Waals loop in comparison to the zero-field case, i.e., ΔT_c is positive. An example of the average projection of $\vec{\mu}/\mu$ onto the direction of the electric field for $\mu = 0.5$ with $\alpha = 0.02$ at $T = 1.10$ is shown in Fig. 5, together with the mean-field result.

TABLE II. ΔT_c and $\Delta\rho_c$ at constant $E^{(\infty)}$ or E^{ext} for $\mu = 0.5$: Simulation results and mean-field (MF) theory.

α	$E^{(\infty)}$	ΔT_c^{sim}	ΔT_c^{MF}	$\Delta\rho_c^{\text{sim}}$	$\Delta\rho_c^{\text{MF}}$
	1.0	0.007	0.006	−0.002	−0.001
	2.0	0.013	0.017	−0.002	−0.001
0.01	3.0	0.032	0.035	−0.004	−0.002
	6.0	0.100	0.099	−0.004	−0.004
	10.0	0.162	0.181	−0.007	−0.005
	1.0	0.009	0.006	< 0.001	0
	2.0	0.023	0.023	−0.002	−0.001
0.02	3.0	0.049	0.047	−0.003	−0.002
	6.0	0.136	0.139	−0.005	−0.004
	10.0	0.245	0.272	−0.010	−0.007
	1.0	0.010	0.010	0.001	−0.001
	2.0	0.039	0.037	< 0.001	−0.002
0.04	3.0	0.075	0.077	−0.003	−0.003
	6.0	0.217	0.240	−0.012	−0.009
	10.0	0.433	0.511	−0.016	−0.013
	1.0	0.018	0.020	0.002	−0.002
	2.0	0.074	0.077	0.002	−0.005
0.08	3.0	0.163	0.162	−0.006	−0.010
	6.0	0.462	0.532	−0.015	−0.022
	10.0	1.101	1.231	−0.027	−0.030
α	E^{ext}	ΔT_c^{sim}	ΔT_c^{MF}	$\Delta\rho_c^{\text{sim}}$	$\Delta\rho_c^{\text{MF}}$
	1.0	−0.006	−0.006	−0.003	0.001
0.01	2.0	−0.023	−0.025	−0.003	0.003
	3.0	−0.051	−0.056	0.004	0.005
	1.0	< 0.001	−0.007	0.001	0.001
0.02	2.0	−0.025	−0.029	0.002	0.004
	3.0	−0.067	−0.067	0.010	0.007
	1.0	−0.008	−0.010	0.002	0.001
0.04	2.0	−0.040	−0.038	0.008	0.005
	3.0	−0.102	−0.087	0.019	0.012
0.08	1.0	−0.013	−0.013	0.005	0.003
	2.0	−0.057	−0.052	0.017	0.011

TABLE III. ΔT_c and $\Delta\rho_c$ at constant $E^{(\infty)}$ or E^{ext} for $\mu = 1.0$: Simulation results and mean-field theory.

α	$E^{(\infty)}$	ΔT_c^{sim}	ΔT_c^{MF}	$\Delta\rho_c^{\text{sim}}$	$\Delta\rho_c^{\text{MF}}$
	1.0	0.022	0.025	−0.006	−0.001
	2.0	0.067	0.084	−0.017	−0.004
0.01	3.0	0.106	0.153	−0.025	−0.006
	6.0	0.248	0.344	−0.032	−0.006
	10.0	0.428	0.548	−0.037	−0.004
	1.0	0.016	0.029	−0.010	−0.001
	2.0	0.070	0.097	−0.021	−0.006
0.02	3.0	0.125	0.178	−0.031	−0.008
	6.0	0.311	0.416	−0.039	−0.010
	10.0	0.542	0.699	−0.043	−0.006
	1.0	0.031	0.037	−0.010	−0.004
	2.0	0.088	0.126	−0.025	−0.010
0.04	3.0	0.166	0.234	−0.037	−0.013
	6.0	0.440	0.581	−0.052	−0.016
	10.0	0.855	1.056	−0.057	−0.014
	1.0	0.032	0.060	−0.018	−0.008
	2.0	0.135	0.202	−0.044	−0.016
0.08	3.0	0.287	0.382	−0.059	−0.021
	6.0	0.884	1.015	−0.076	−0.024
	10.0	1.962	2.027	−0.074	−0.021
α	E^{ext}	ΔT_c^{sim}	ΔT_c^{MF}	$\Delta\rho_c^{\text{sim}}$	$\Delta\rho_c^{\text{MF}}$
0.01	1.0	−0.015	−0.014	0.010	0.004
	2.0	−0.078	−0.055	0.024	0.019
0.02	1.0	−0.016	−0.014	0.008	0.007
	2.0	−0.059	−0.056	0.028	0.022
0.04	1.0	−0.011	−0.015	0.006	0.002
	2.0	−0.062	−0.056	0.035	0.019
0.08	1.0	−0.017	−0.015	0.011	0.005
	2.0	−0.048	−0.056	0.034	0.025

At this point a discussion about errors affecting our results thus far is in order. The critical parameters are obtained in several steps, contributing differently to the overall error: (i) Acquisition of isotherms via standard *NVT* MD—the results are affected by system size and interaction cutoff; (ii) fitting of isotherm data with a phenomenological equation of state to obtain the densities at coexistence; and (iii) scaling law fitting of coexistence data using the exponents of the Ising universality class. Mainly due to the intermittent fitting, it is difficult to compute a standard mean error in the sense that the attendant error bar brackets the true value to within a certain probability.

An alternative is the explicit inspection of coexistence data, i.e., the scatter of the data points for independent conditions and/or different parameter values, for different field strengths and/or polarizabilities (as in Fig. 3). This type of data provides a measure for the resolution of the method in terms of field strength and polarization. On the level of the coexistence curves the error is comparable to the symbol size, which means ∼0.3% in case of the critical temperature. The respective error for the critical density is larger—∼1% to 2%—due to the flatness of the coexistence curve. Nevertheless, Fig. 2 (top) shows that the critical temperatures of completely independent simulations for different polarizations at a fixed permanent dipole moment show little scatter and are in very good agreement with results from other groups using other computational methods (and system sizes). The attendant critical densities are less certain, but our own independent results for fixed permanent dipole moments but with variable polarizabilities may still be represented by a smooth curve to within the width of the symbols. Here the deviation from the literature data, which are not entirely consistent, might be due to a systematic error either in our own analysis or that of the literature data.

The finite-size scaling analysis for the heat capacity in Fig. 7 (bottom panel), discussed below and, not to be confused with the effect due to the cutoff of critical fluctuations as shown in the top panel, shows that the result for $N = 900$, the standard size, differs from the extrapolation to infinite system size by ∼0.5% in the worst case. If we carry this over to the critical temperature and the critical density, which should behave similarly, we obtain errors comparable to the numbers quoted above. The finite-size error, however, will be essentially

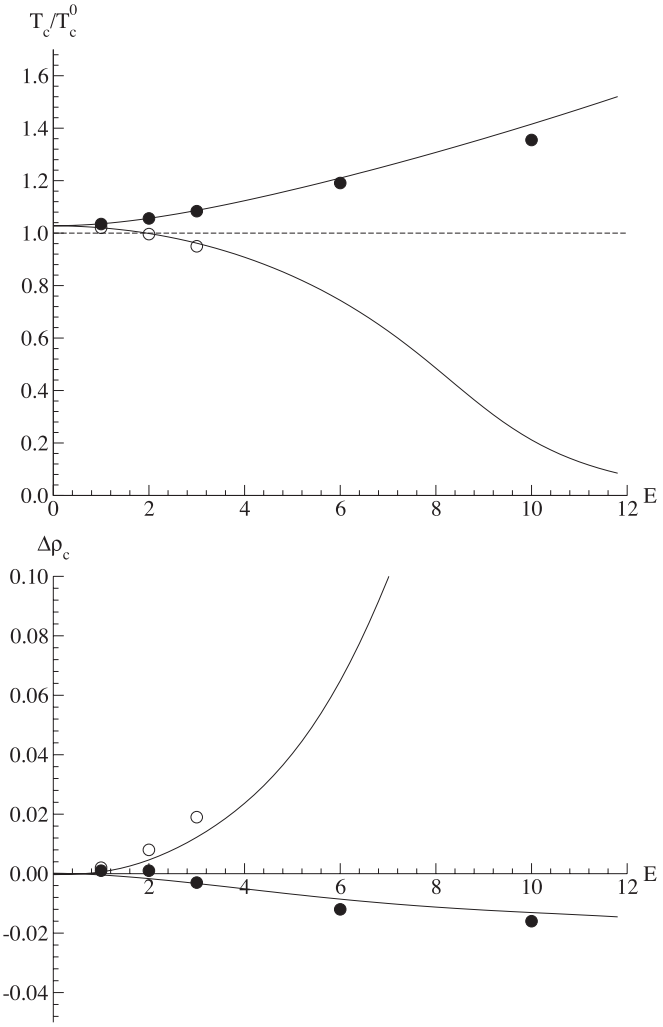

FIG. 4. Top: Mean-field critical temperature in units of the LJ critical temperature vs E (specified for each curve). Bottom: Mean-field critical density shift vs E. Both are plotted for $\mu = 0.5$ and $\alpha = 0.04$ with $r_{\rm cut} = 0.8$; LJ critical density $\rho_c^0 = 0.3$; LJ critical temperature $T_c^0 = 1.32$. Symbols are simulation results. Solid circles: $E = E^{(\infty)}$; open circles: $E = E^{\rm ext}$. The statistical error again is comparable to the size of the symbols.

subtracted out of the differences tabulated in Tables I, II, and III. Overall we conclude that the differences given in the tables are subject to considerable uncertainty for small polarizability and small field strength, but the trends described by this set of data as a whole are reliable.

Figure 6 shows the isochoric heat capacity per particle C_V/N versus number density ρ for the nonpolarizable ST system with $\mu = 1.0$ in the absence of an external field at selected temperatures. As an independent check of our simulation data we use the thermodynamic relation $\partial C_V/\partial V\,|_T = T\,\partial^2 P_V/\partial T^2\,|_V$ to obtain the low-density approximation $C_V - C_V^{\rm ideal} = -N\rho T[2\frac{\partial}{\partial T}B_2^{\rm ST} + T\frac{\partial^2}{\partial T^2}B_2^{\rm ST}]$. Here $B_2^{\rm ST}$ is the second virial coefficient of the ST fluid (cf. the Appendix of Ref. [24]). The inset in Fig. 6 shows the comparison between our simulations and this theoretical result.

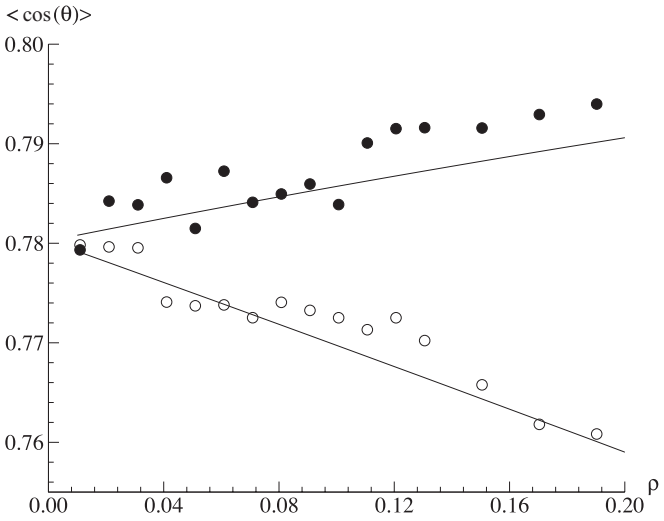

FIG. 5. Average orientation of the dipoles relative to the electric field direction $\langle\cos\theta\rangle$ vs density ρ for $\mu = 0.5$, $\alpha = 0.02$, and $T = 1.10$. Solid lines: mean-field theory; solid circles: simulation result for $E^{(\infty)} = 10$; open circles: simulation result for $E^{\rm ext} = 10$.

It is interesting to study finite-size dependence of the peak at criticality. The expected scaling is

$$\ln\frac{C_V}{N} = \frac{1}{3}\frac{\alpha}{\nu}\ln N + \text{const.} \tag{7}$$

This follows via $C_V \sim |T - T_c|^{-\alpha}$ in conjunction with $N^{1/3} \sim \xi \sim |T - T_c|^{-\nu}$, where ξ is the (energy-energy) fluctuation correlation length and α and ν are critical exponents. Figure 7 shows a plot of $\ln C_v/N$ vs $\ln N$ with a slope $\approx$0.060. This is in rather good accord with the expected three-dimensional (3D) Ising value $\alpha/(3\nu) = 0.058$ (e.g., Ref. [26]). However, our value of 0.060 should be corrected for the finite-size

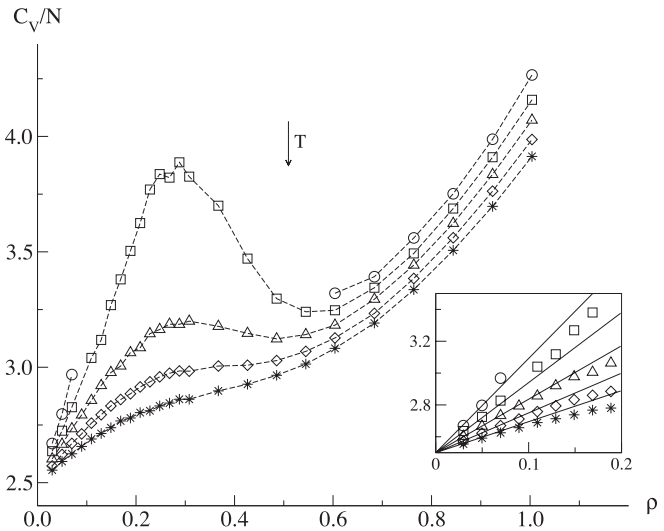

FIG. 6. Isochoric heat capacity per particle C_V/N vs particle number density ρ in the absence of an external field. The symbols (joined by dashed lines) are simulation results for $\mu = 1$, $\alpha = 0$, $r_{\rm cut} = 4.0$. From top to bottom: $T = 1.3, 1.445, 1.6, 1.8, 2.0$. For the subcritical temperature the curves terminate on the coexistence curve. The inset shows a low-density comparison between the simulation results and a second-order virial expansion (solid lines).

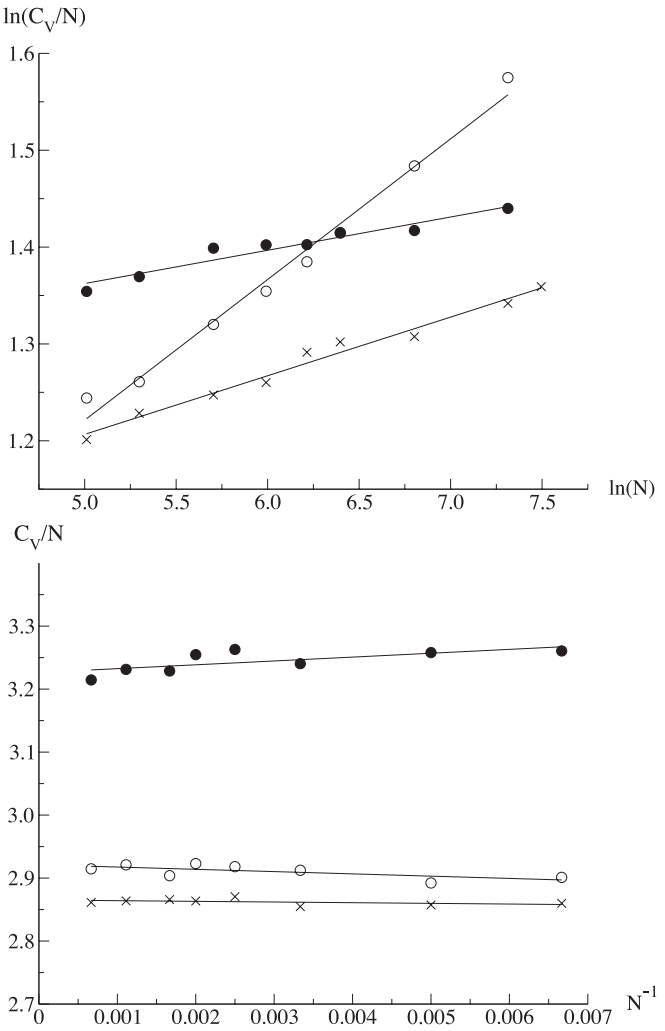

FIG. 7. Top: Critical finite-size scaling for C_V/N of a ST system with $\mu = 1.0$. Symbols are simulation results. Crosses: $E = 0$ ($T = 1.445$, $\rho = 0.309$); solid circles: $E^{(\infty)} = 2$ ($T = 1.502$, $\rho = 0.297$); open circles: $E^{\text{ext}} = 2$ ($T = 1.388$, $\rho = 0.331$). Lines are least-squares approximations. Bottom: Scaling of C_V/N vs N^{-1} for the ST system with $\mu = 1.0$ at $T = 2.0$, which is far from the respective critical temperatures. The meaning of the symbols and lines is the same as above.

dependence of C_V far from criticality. The bottom part shows a plot C_V/N vs $1/N$, i.e., the expected dependence on N in this case. If the same data are plotted in the form of the upper panel (not shown here), one finds that the resulting slope is $\sim$10% of 0.060, which would mean that our resulting estimate of $\alpha/(3\nu)$ is close to 0.054. Similar numbers are obtained for nonzero polarizability.

The presence of an external field alters this behavior. The two results in Fig. 7 for $\vec{E}^{(\infty)} = 2$ and $\vec{E}^{\text{ext}} = 2$ show distinctly different slopes. For $E^{(\infty)} = 2$ the ST fluid exponent $\alpha/(3\nu)$ is $\sim$40% smaller than the 3D Ising value. In the other case, i.e., $E^{\text{ext}} = 2$, we obtain an exponent for the ST fluid which exceeds the 3D Ising value by a factor of 2.5. We emphasize that we still talk about the gas-liquid critical point and not about the ferroelectric transition also observed on the ST fluid. However, we are not aware of a discussion of (electric) field effects on critical exponent values in the case of gas-liquid criticality in the presence of (electric) fields.

Exponent values essentially depend on order parameter symmetry, space dimension, and range of interactions (long versus short) (e.g., Ref. [27]). The range of interparticle interactions may be affected by the formation of reversible aggregates, i.e., possibly long chains, commonly observed in dipolar fluids depending on thermodynamic conditions (e.g., Ref. [23]). However, the (small) mean aggregation numbers, using a simple distance criterion, are identical to within the scatter in the cases $E = 0$ and $E^{(\infty)} = 2$. It is slightly increased in the case $E^{\text{ext}} = 2$. Therefore, in the present case is not likely that aggregate formation significantly increases the interaction range and causes an attendant approach to mean-field behavior. The latter would lead to a strongly decreased or (ideally) zero slope, which would be in line with the $E^{(\infty)} = 2$ result but certainly not with the $E^{\text{ext}} = 2$ result. We note that we have monitored clustering or aggregation throughout this paper and have only included results when we could not detect aggregation (e.g., the case $\mu = 2.0$, $\alpha = 0.08$ is excluded from Table I for this reason). Another thought might be the following. Anisotropic interactions (in, for instance, magnetic systems) lead to an effective decrease of dimension. The orientational ordering imposed by a nonzero field certainly causes anisotropy. Even though the resulting anisotropy is different for $E^{(\infty)} > 0$ in comparison to $E^{\text{ext}} > 0$, as shown in Fig. 5, this effect appears insufficient to cause the opposite deviation of slopes relative to the $E = 0$ result. Because this is a simulation, where critical parameters are determined approximately (and rather crudely), unaccounted for corrections to the leading scaling behavior may affect the observed slopes and cause opposite deviations from the zero-field slope.

IV. CONCLUSION

Using the MD technique we compute gas-liquid phase coexistence curves for the pST fluids in external fields. In order to avoid the formation of reversible aggregates, which complicate matters considerably, we have studied mainly small permanent dipole moments and polarizabilities. Our mean-field description for small polar molecules including induced polarization is in good accord with the simulation results, except for the critical parameter ratios when $E = 0$ and $\alpha \neq 0$. The shift of the critical point as function of electric field strength is obtained for the case of fixed external charge density or fixed potential. As before, for the nonpolarizable ST [5], we observe a decrease of T_c in the former case and an increase in the latter. Increasing the polarizability is analogous to increasing the permanent dipole moment. The critical density behaves more subtly. This is seen in the case of vanishing field strength. Depending on the size of the permanent dipole moment, there may be a shift, increasing with increasing polarizability, in both directions. Via analysis of the isochoric heat capacity using simple finite-size scaling, we estimate the exponent ratio α/ν at vanishing field strength. The resulting value is in accord with the expected Ising behavior. In the two cases of non-zero-field strength we observe apparent deviations. For fixed external charge density α/ν is increased, whereas in the fixed potential case it is decreased.

[1] W. H. Stockmayer, J. Chem. Phys. **9**, 398 (1941); however, Stockmayer was not the first to study simple intramolecular potentials with (electrostatic) dipolar interactions. He also uses a r^{-s} repulsion with $s = 24$ instead of $s = 12$, which is the common power today.
[2] M. A. Pounds and P. A. Madden, J. Chem. Phys. **126**, 104506 (2007).
[3] J.-J. Weis and D. Levesque, in *Advanced Computer Simulation Approaches for Soft Matter Sciences II*, edited by C. Holm and K. Kremer, Advances in Polymer Science, Vol. 185 (Springer, New York, 2005).
[4] S. H. L. Klapp, J. Phys. Condens. Matter **17**, R525 (2005).
[5] R. Jia and R. Hentschke, Phys. Rev. E **80**, 051502 (2009).
[6] F. J. Vesely, J. Comput. Phys. **24**, 361 (1977).
[7] F. J. Vesely, Chem. Phys. Lett. **56**, 390 (1978).
[8] S. L. Carnie and G. N. Patey, Mol. Phys. **47**, 1129 (1982).
[9] J. M. Caillol, D. Levesque, J. J. Weis, P. G. Kusalik, and G. N. Patey, Mol. Phys. **55**, 65 (1985).
[10] G. N. Patey, D. Levesque, and J. J. Weis, Mol. Phys. **57**, 337 (1986).
[11] M. Neumann and O. Steinhauser, Chem. Phys. Lett. **106**, 563 (1984).
[12] G. C. A. M. Mooij, S. W. de Leeuw, C. P. Williams, and B. Smit, Mol. Phys. **71**, 909 (1990).
[13] G. C. A. M. Mooij, S. W. de Leeuw, B. Smit, and C. P. Williams, J. Chem. Phys. **97**, 5113 (1992).
[14] C. Kriebel and J. Winkelmann, Mol. Phys. **88**, 559 (1996).
[15] C. Millot, J. C. Soetens, and M. T. C. Martins Costa, Mol. Simul. **18**, 367 (1997).
[16] M. Valiskó, D. Boda, J. Liszi, and I. Szalai, Mol. Phys. **101**, 2309 (2003).
[17] M. Valiskó and D. Boda, Condens. Matter Phys. **8**, 357 (2005).
[18] F. Moučka, M. Rouha, and I. Nezbeda, J. Chem. Phys. **126**, 224106 (2007).
[19] C. Kriebel and J. Winkelmann, Mol. Phys. **90**, 297 (1997).
[20] K. Kiyohara, K. E. Gubbins, and A. Z. Panagiotopoulos, J. Chem. Phys. **106**, 3338 (1997).
[21] H. Fröhlich, *Theory of Dielectrics* (Oxford University Press, London, 1958).
[22] H. J. C. Berendsen, J. P. M. Postma, W. F. van Gunsteren, A. DiNola, and J. R. Haak, J. Chem. Phys. **81**, 3684 (1984).
[23] R. Hentschke, J. Bartke, and F. Pesth, Phys. Rev. E **75**, 011506 (2007).
[24] J. Bartke and R. Hentschke, Phys. Rev. E **75**, 061503 (2007).
[25] J. Bartke and R. Hentschke, Mol. Phys. **104**, 3057 (2006).
[26] A. Pelissetto and E. Vicari, Phys. Rep. **368**, 549 (2002).
[27] M. E. Fisher, Rev. Mod. Phys. **46**, 597 (1974).